Electronic Supplementary Material (ESI) for Soft Matter.

Supplementary Information

Intrinsic structure and dynamics of monolayer ring polymer melts

Jinseong Kim[a,‡], Jun Mo Kim[b,‡], and Chunggi Baig[a,*]

[a]*School of Energy and Chemical Engineering, Ulsan National Institute of Science and Technology (UNIST), UNIST-gil 50, Eonyang-eup, Ulju-gun, Ulsan 44919, South Korea*

[b]*Department of Chemical Engineering, Kyonggi University, 154-42 Gwanggyosan-ro, Yeongtong-gu, Suwon, Kyonggi-do 16227, South Korea*

[‡]These authors contributed equally to this work

[*]Corresponding Author. Email: cbaig@unist.ac.kr

Simulation methodology

Atomistic molecular dynamics simulation

We simulated the monodisperse (unconcatenated and unknotted) ring polyethylene (PE) melts via atomistic canonical (*NVT*) molecular dynamics (MD) method at constant temperature (*T* = 450 K) and density (corresponding to the pressure *P* = 1 atm) by using the set of the equations of motion, implemented with the Nosé–Hoover thermostat:[1-3]

$$\dot{\mathbf{q}}_{ia} = \frac{\mathbf{p}_{ia}}{m_{ia}}$$

$$\dot{\mathbf{p}}_{ia} = \mathbf{F}_{ia} - \dot{\varsigma}\mathbf{p}_{ia} \tag{1}$$

$$\dot{\varsigma} = \frac{p_{\varsigma}}{Q}, \quad p_{\varsigma} = \sum_i \sum_a \frac{p_{ia}^2}{m_{ia}} - DNk_BT, \quad Q = DNk_BT\tau^2$$

where $\mathbf{q}_{ia}$, $\mathbf{p}_{ia}$, and $\mathbf{F}_{ia}$ are, respectively, the position, momentum, and force vectors of atom *a* in molecule *i* of mass m_{ia}. *D* denotes the dimensionality of the system and k_B the Boltzmann constant. *N* and *V* represent the total number of atoms and the volume of the system, respectively. ς and p_{ς} are the coordinate- and momentum-like variables, respectively, of the Nosé–Hoover thermostat. *Q* is the mass parameter of the thermostat. The thermostat relaxation time parameter τ was set equal to 0.12 ps for all simulations The set of equations of motion in the atomistic MD simulation were numerically integrated using the efficient reversible Reference System Propagator Algorithm (*r*-RESPA)[4] with two distinct time scales: a short time scale of 0.47 fs for three bonded (bond-stretching, bond-bending, and bond-torsional) interactions and a long time scale of 2.35 fs for nonbonded intramolecular and intermolecular Lennard–Jones (LJ) interactions.

The well-known Siepmann-Karaboni-Smit (SKS) united-atom model[5] was adopted for all the atomistic simulations because of its broad usage and accuracy for predicting structural and dynamical properties of linear alkanes. In this model, the nonbonded intermolecular and intramolecular interactions between atomic units are described by a standard 6-12 LJ potential:

$$U_{\mathrm{LJ}}(r) = 4\varepsilon_{ij}\left[\left(\frac{\sigma_{ij}}{r_{ij}}\right)^{12} - \left(\frac{\sigma_{ij}}{r_{ij}}\right)^{6}\right] \tag{2}$$

where $\varepsilon_{ij} = \sqrt{\varepsilon_i \varepsilon_j}$ and $\sigma_{ij} = (\sigma_i + \sigma_j)/2$ for cross interactions between atoms *i* and *j* by adopting the standard Lorentz-Berthelot mixing rules. r_{ij} is the distance between atoms *i* and *j*. For the CH_2 united atom in ring polyethylene (PE) molecules, the LJ energy parameter $\varepsilon_{\mathrm{CH_2}}/k_B$ was equal to 47 K, and the LJ size parameter $\sigma_{\mathrm{CH_2}}$ was equal to 3.93 Å. A cut-off distance equal to $2.5\sigma_{\mathrm{CH_2}}$ was used in all simulations. The intramolecular LJ interaction was active only between atoms separated by more than three bonds along the chain.

The bond-stretching interaction is described by harmonic potential:

$$U_{\mathrm{stretching}}(l) = \frac{k_{\mathrm{str}}}{2}(l - l_{\mathrm{eq}})^2 \tag{3}$$

with the equilibrium bond length l_{eq} = 1.54 Å and bond-stretching constant k_{str}/k_B = 452,900 K/Å^2. The bond-bending interaction is also applied based on a harmonic potential:

$$U_{\mathrm{bending}}(\theta) = \frac{k_{\mathrm{ben}}}{2}(\theta - \theta_{\mathrm{eq}})^2 \tag{4}$$

with the equilibrium bending angle θ_{eq} = 114° and bond-bending constant k_{ben}/k_B = 62,500 K/

rad[2] based on van der Ploeg *et al*.[6]. The bond-torsional interaction is governed by the potential by Jorgensen *et al*.:[7]

$$U_{\text{torsional}}(\phi) = \sum_{m=0}^{3} a_m \cos^m \phi \tag{5}$$

with the bond-torsional constants a_0/k_B = 1010 K, a_1/k_B = 2019 K, a_2/k_B = 136.4 K and a_3/k_B = – 3165 K.

The nearly 2D confined atomistic systems employed in this study were constructed by placing two simple rigid, repulsive walls which simply do not allow polymer chains to move out of the boundary walls. This allows us to focus on the general, fundamental characteristics of polymeric systems under extreme confinement, without regard to the specific polymer-wall interactions. The repulsive wall was described by the Weeks-Chandler-Anderson (WCA) potential:[8]

$$U_{\text{LJ}}(r) = \begin{cases} 4\varepsilon_{i\text{w}}\left[\left(\dfrac{\sigma_{i\text{w}}}{r_{i\text{w}}}\right)^{12} - \left(\dfrac{\sigma_{i\text{w}}}{r_{i\text{w}}}\right)^{6}\right] + \varepsilon_{i\text{w}}, & r_{i\text{w}} \le 2^{1/6}\sigma_{i\text{w}} \\ 0, & r_{i\text{w}} > 2^{1/6}\sigma_{i\text{w}} \end{cases} \tag{6}$$

where $\sigma_{i\text{W}} = \sigma_{\text{CH}_2}/2$, $\varepsilon_{i\text{W}}/k_B$ = 47 K, and $r_{i\text{w}}$ is the distance between atom *i* and wall surface.

The system density was determined by additional atomistic isothermal-isobaric (*NPT*) MD simulations at constant temperature (T = 450 K) and pressure (P = 1 atm) using the Nosé-Hoover thermostat and barostat with their relaxation time parameters being set equal to 0.12 ps.

Coarse-grained Kremer-Grest (KG) simulation

NVT coarse-grained (CG) KG simulations of the monodisperse (unconcatenated and unknotted) ring melt systems were conducted at constant temperature $T = \varepsilon_{\mathrm{KG}} / k_B$ using Langevin thermostat and a constant area for the strictly 2D systems. The equations of motion for the position vectors implemented with the Langevin thermostat for Canonical KG MD simulations[9] are as follows:

$$m\ddot{\mathbf{r}}_i = \mathbf{F}_i - \Gamma\dot{\mathbf{r}}_i + \mathbf{W}_i(t) \tag{7}$$

where $\mathbf{r}_i$ and $\mathbf{F}_i$ are the position and force vectors of bead *i*, respectively. The bead friction coefficient was set as $\Gamma = 0.5\ \tau_{\mathrm{KG}}^{-1}$ at constant temperature $T = \varepsilon_{\mathrm{KG}} / k_B$. $\mathbf{W}_i(t)$ denotes the Gaussian white noise source with zero mean at a temperature *T* and satisfies the standard fluctuation-dissipation relation for 2D systems: $< \mathbf{W}_i(t) \cdot \mathbf{W}_j(t') >= 4\delta_{ij}\delta(t-t')\Gamma k_B T$.

The KG simulations were carried out with the four (intermolecular, intramolecular, bond-stretching, and bond-bending) interaction potentials. Shifted LJ (WCA) potential function is applied to calculate intermolecular and intramolecular interactions between beads:

$$U_{\mathrm{LJ}}^{\mathrm{KG}}(r) = \begin{cases} 4\varepsilon_{\mathrm{KG}}\left[\left(\dfrac{\sigma_{\mathrm{KG}}}{r_{ij}}\right)^{12} - \left(\dfrac{\sigma_{\mathrm{KG}}}{r_{ij}}\right)^{6}\right] + \varepsilon_{\mathrm{KG}}, & r_{ij} \le 2^{1/6}\sigma_{\mathrm{KG}} \\ 0, & r_{ij} > 2^{1/6}\sigma_{\mathrm{KG}} \end{cases} \tag{8}$$

where σ_{KG} and $\varepsilon_{\mathrm{KG}}$ are the LJ bead size and energy parameters, respectively. r_{ij} denotes the distance between beads *i* and *j*. The cut-off distance is set as $r_c = 2^{1/6}\sigma_{\mathrm{KG}}$. The bond-stretching interaction is described by the finitely extensible nonlinear elastic (FENE) potential:

$$U_{\mathrm{FENE}}^{\mathrm{KG}}(r)=\begin{cases}-\frac{1}{2}kR_0^2\ln[1-(r_{ij}/R_0)^2], & r_{ij}\le R_0\\ \infty, & r_{ij}>R_0\end{cases} \tag{9}$$

with the maximum bond length $R_0 = 1.5\,\sigma_{\mathrm{KG}}$ and bond-stretching constant $k = 30\,\varepsilon_{\mathrm{KG}}/\sigma_{\mathrm{KG}}^2$.[9] r_{ij} is the distance between the two neighboring beads i and $j=i+1$. The bond-bending interaction is given by

$$U_{\mathrm{bending}}^{\mathrm{KG}}(\theta_i)=k_\theta[1-\cos\theta_i] \tag{10}$$

with the bond-bending constant $k_\theta = 0$, $k_\theta = 3$, and $k_\theta = 4$, and the bending angle θ_i between the two consecutive bond vectors $\vec{\mathbf{b}}_i = \vec{\mathbf{r}}_i - \vec{\mathbf{r}}_{i-1}$ and $\vec{\mathbf{b}}_{i+1} = \vec{\mathbf{r}}_{i+1} - \vec{\mathbf{r}}_i$.[10,11]

Supplementary Note 1

As shown in our previous[15] and present studies, polymer chains, when narrowly confined or at interfaces, intrinsically attain a certain degree of chain stiffness. Fundamentally, this change in chain flexibility stems from an entropic penalty in association with the reduction in available chain configurational states by geometric constraint. However, the existing theoretical and numerical models (e.g., the Rouse model and the standard KG model) for dense 2D linear and ring polymer systems are, as essentially similar to the models for the corresponding 3D systems, based on the random walk or self-avoiding random walk (SAW) of individual chain segments without properly accounting for the naturally arising chain stiffness caused by dimensional restriction in 2D space. Accordingly, those theoretical analyses based on random-walk chain models for 2D or very narrowly confined systems[12,13] are likely to result in physically incorrect results. For instance, the Rouse model and the standard KG model including de Gennes's analysis give rise to the compact segregated chain configurations for 2D concentrated polymer solutions or melts of general flexible polymers, which is in sharp contradiction to the extended interpenetrated chain configurations attained by our direct 2D atomistic simulations and available interfacial experiments such as monolayer Langmuir polymer films.[14] Also, the atomistic results in Fig. 2 clearly refute the Rouse model prediction of $\left\langle R_{\mathrm{g}}^2 \right\rangle_{\mathrm{Ring}} = \left\langle R_{\mathrm{g}}^2 \right\rangle_{\mathrm{Linear}} / 2$ for 2D confined melt systems of the same chain length. Further, the atomistic simulations exhibit a non-Gaussian probability distribution $P\left(\left|\mathbf{R}_{\mathrm{ete}}\right|\right)$ of the chain end-to-end distance $\left|\mathbf{R}_{\mathrm{ete}}\right|$ for the 2D linear melt systems,[15] in stark contrast to the typical Gaussian behavior predicted by the random-walk based Rouse model and standard KG model. In addition, while the atomistic simulations show approximately a Rouse-like scaling behavior with $\tau_{\mathrm{Relax}} \sim N^2$ for the 2D linear and ring PE melts, they invalidate the Rouse

model prediction for the value of $(\tau_{\text{Relax}})_{\text{Ring}} = (\tau_{\text{Relax}})_{\text{Linear}}/4$. Furthermore, as shown in Fig. 7, the standard 2D KG model with $k_\theta = 0$ (without accounting for the naturally arising chain stiffness due to dimensional constraints) produce generally inconsistent results for the main structural and dynamical properties in comparison to those obtained from the direct 2D atomistic simulations.

In addition, as shown below, the direct 2D atomistic simulations show some deviations for scaling behaviors of structural and dynamical properties in comparison to the theoretical results by A. N. Semenov and A. Johner[13] for monolayer linear polymer melts.

	Semenov-Johner model[13]	2D atomistic result[15]
$\langle R_g^2 \rangle$	N	$N^{0.97\pm0.03}$
L (perimeter monomer)	$N^{0.625}$	$N^{0.80\pm0.03}$
D_G	$N^{-0.875}$	$N^{-0.96\pm0.04}$
τ_{Relax}	$N^{1.875}$	$N^{1.92\pm0.10}$

Supplementary Note 2

Two-dimensional (2D) Rouse model for linear and ring polymers

Here we present a detailed analysis of the 2D Rouse model of linear and ring polymers. The derivation is essentially similar to that of the corresponding three-dimensional (3D) model.[16] As standard, the effect of hydrodynamic interactions is not included in this analysis, which thus, based on the mean-field concept, refers to short unentangled polymer melt systems. Each chain is composed of N coarse-grained beads with an effective hydrodynamic friction coefficient ζ, which are connected by Gaussisan springs of the equilibrium length b and spring constant $K = 2k_BT/b^2$ for 2D systems where k_B is the Boltzmaan constant and T the temperature. The dynamics of an N-bead Rouse chain under equilibrium conditions can be decribed by the following Langevin eqation:

$$\zeta \frac{\partial \mathbf{R}_n}{\partial t} = -\frac{\partial U}{\partial \mathbf{R}_n} + \mathbf{f}_n(t) \quad \text{for } n = 1, 2, \cdots, N \tag{11}$$

where U represents the harmonic poetential energy of the Gaussisan springs:

$$U = \frac{K}{2} \sum_{n=1}^{N-1} (\mathbf{R}_{n+1} - \mathbf{R}_n)^2 \tag{12}$$

Here $\mathbf{R}_n$ denotes the position vector of the n^{th} bead and $\mathbf{f}_n(t)$ is the random Brownian force exerted on this bead. The $\mathbf{f}_n(t)$ obeys the following eqations:

$$\langle \mathbf{f}_n(t) \rangle = 0 \tag{13a}$$

$$\langle f_{n\alpha}(t) f_{m\beta}(t') \rangle = 2\zeta k_B T \delta_{mn} \delta_{\alpha\beta} \delta(t - t') \text{ for } \alpha, \beta = x, y \tag{13b}$$

where δ_{mn} is the Kronecker delta and $\delta(t - t')$ denotes the Direc delta function. Combining eqns

(1) and (2), we obtain this equation:

$$\zeta \frac{\partial \mathbf{R}_n}{\partial t} = K \frac{\partial^2 \mathbf{R}_n}{\partial n^2} + \mathbf{f}_n(t) \tag{14}$$

The boundary conditions for the 2D linear polymer are as follows:

$$\left.\frac{\partial \mathbf{R}_n}{\partial n}\right|_{n=0} = 0 \,,\ \left.\frac{\partial \mathbf{R}_n}{\partial n}\right|_{n=N} = 0 \tag{15}$$

On the other hand, the boundary conditions for the 2D ring polymer are as follows:

$$\mathbf{R}_0 = \mathbf{R}_N \,,\ \left.\frac{\partial \mathbf{R}_n}{\partial n}\right|_{n=0} = \left.\frac{\partial \mathbf{R}_n}{\partial n}\right|_{n=N} \tag{16}$$

To conveniently solve the Rouse model, we can employ the normal coordinates $\mathbf{X}_p(t)$ and $\mathbf{Y}_p(t)$ through

$$\mathbf{R}_n(t) = \mathbf{X}_0 + \sum_{p=1}^{\infty} \left[2\mathbf{X}_p \cos(\frac{p\pi n}{N}) + 2\mathbf{Y}_p \sin(\frac{p\pi n}{N}) \right] \tag{17a}$$

$$\mathbf{X}_p(t) = \frac{1}{N} \int_0^N \mathbf{R}_n(t) \cos(\frac{p\pi n}{N}) \mathrm{d}n \ \text{ for } p = 0, 1, 2, 3, 4, \ldots \tag{17b}$$

$$\mathbf{Y}_p(t) = \frac{1}{N} \int_0^N \mathbf{R}_n(t) \sin(\frac{p\pi n}{N}) \mathrm{d}n \ \text{ for } p = 1, 2, 3, 4, \ldots \tag{17c}$$

Applying the boundary conditions (eqn (5)) to eqn (7a), we find the following result for the linear polymer:

$$\mathbf{R}_n(t) = \mathbf{X}_0 + \sum_{p;even}^{\infty} \left[2\mathbf{X}_p \cos(\frac{p\pi n}{N}) + 2\mathbf{Y}_p \sin(\frac{p\pi n}{N}) \right] \tag{18a}$$

$$\mathbf{X}_p(t) = \frac{1}{N}\int_0^N \mathbf{R}_n(t)\cos(\frac{p\pi n}{N})\mathrm{d}n \ \text{ for } p = 0, 1, 2, 3, 4, \ldots \tag{18b}$$

$$\mathbf{Y}_p(t) = 0 \ \text{ for } p = 1, 2, 3, 4, \ldots \tag{18c}$$

By applying the boundary conditions (eqn (6)) to eqn (7a), we find the following result for the ring polymer:

$$\mathbf{R}_n(t) = \mathbf{X}_0 + \sum_{p;even}^{\infty}\left[2\mathbf{X}_p\cos(\frac{p\pi n}{N}) + 2\mathbf{Y}_p\sin(\frac{p\pi n}{N})\right] \tag{19a}$$

$$\mathbf{X}_p(t) = \frac{1}{N}\int_0^N \mathbf{R}_n(t)\cos(\frac{p\pi n}{N})\mathrm{d}n \ \text{ for } p = 0, 2, 4, 6, \ldots \tag{19b}$$

$$\mathbf{Y}_p(t) = \frac{1}{N}\int_0^N \mathbf{R}_n(t)\sin(\frac{p\pi n}{N})\mathrm{d}n \ \text{ for } p = 2, 4, 6, 8, \ldots \tag{19c}$$

where *p;even* in the summation represents only the even *p*-modes, i.e., $p = 2, 4, 6, 8\cdots$. Note that all the odd modes should vanish for ring polymers.

In terms of the normal coordinates, the set of the Langevin equation (eqn (1)) for the 2D linear polymer can be equivalently written as

$$2N\zeta\frac{\partial \mathbf{X}_p}{\partial t} = -k_p\mathbf{X}_P + \mathbf{f}_p^X \tag{20a}$$

$$\mathbf{f}_p^X = 2\int_0^N \mathbf{f}_n(t)\cos(\frac{p\pi n}{N})\mathrm{d}n \ \text{ for } p = 0, 1, 2, 3, 4, \ldots \tag{20b}$$

where

$$k_p = \frac{4\pi^2 k_B T}{Nb^2} p^2 \quad \text{for } p = 0, 1, 2, 3, 4, \ldots \tag{21}$$

Using eqn (3), we also find

$$\left\langle \mathbf{f}_p^X(t) \right\rangle = 0 \tag{22a}$$

$$\left\langle f_{p\alpha}^X(t) f_{q\beta}^X(t') \right\rangle = 4N\zeta k_B T \delta_{pq} \delta_{\alpha\beta} \delta(t-t') \quad \text{for } p \neq 0 \text{ or } q \neq 0 \tag{22b}$$

$$\left\langle f_{0\alpha}^X(t) f_{0\beta}^X(t') \right\rangle = 8N\zeta k_B T \delta_{\alpha\beta} \delta(t-t') \tag{22c}$$

Solving eqn (10a) for $\mathbf{X}_p$, we find

$$\mathbf{X}_p(t) = \frac{1}{2N\zeta} \int_{-\infty}^{t} \mathbf{f}_p^X(t') \exp\left[-(t-t')/\tau_p\right] \mathrm{d}t' \quad p = 0, 1, 2, 3, 4, \ldots \tag{23}$$

where

$$\tau_p = \frac{\zeta N^2 b^2}{2\pi^2 k_B T} \frac{1}{p^2} \quad \text{for } p = 1, 2, 3, 4, \ldots \tag{24}$$

Using eqn (12), we then obtain

$$\left\langle X_{p\alpha}(t) X_{q\beta}(0) \right\rangle = \delta_{pq} \delta_{\alpha\beta} \frac{k_B T}{k_p} \exp\left(-t/\tau_p\right) \quad \text{for } p, q = 1, 2, 3, 4, \cdots \tag{25}$$

Similarly, the set of the Langevin equation (eqn (1)) for the 2D ring polymer can be equivalently written as

$$2N\zeta \frac{\partial \mathbf{X}_p}{\partial t} = -k_p \mathbf{X}_P + \mathbf{f}_p^X \tag{26a}$$

$$\mathbf{f}_p^X = 2\int_0^N \mathbf{f}_n(t)\cos(\frac{p\pi n}{N})\mathrm{d}n \text{ for } p = 0, 2, 4, 6, \ldots \quad (26b)$$

$$2N\zeta\frac{\partial \mathbf{Y}_p}{\partial t} = -k_p\mathbf{Y}_P + \mathbf{f}_p^Y \quad (26c)$$

$$\mathbf{f}_p^Y = 2\int_0^N \mathbf{f}_n(t)\sin(\frac{p\pi n}{N})\mathrm{d}n \text{ for } p = 2, 4, 6, 8, \ldots \quad (26d)$$

where

$$k_p = \frac{4\pi^2 k_B T}{Nb^2}\, p^2 \text{ for } p = 0, 2, 4, 6, \ldots \quad (27)$$

Using eqn (3), we also find

$$\left\langle \mathbf{f}_p^X(t)\right\rangle = \left\langle \mathbf{f}_p^Y(t)\right\rangle = 0 \quad (28a)$$

$$\left\langle f_{p\alpha}^X(t) f_{q\beta}^X(t')\right\rangle = \left\langle f_{p\alpha}^Y(t) f_{q\beta}^Y(t')\right\rangle = 4N\zeta k_B T\delta_{pq}\delta_{\alpha\beta}\delta(t-t') \text{ for } p \neq 0 \text{ or } q \neq 0 \quad (28b)$$

$$\left\langle f_{0\alpha}^X(t) f_{0\beta}^X(t')\right\rangle = 8N\zeta k_B T\delta_{\alpha\beta}\delta(t-t') \quad (28c)$$

$$\left\langle f_{p\alpha}^X(t) f_{q\beta}^Y(t')\right\rangle = 0 \text{ for all } p \text{ and } q \quad (28d)$$

Solving eqns (16a) for $\mathbf{X}_p$ and (16c) for $\mathbf{Y}_p$, we find

$$\mathbf{X}_P(t) = \frac{1}{2N\zeta}\int_{-\infty}^t \mathbf{f}_p^X(t')\exp\left[-(t-t')/\tau_p\right]\mathrm{d}t' \; p = 0, 2, 4, 6, \ldots \quad (29a)$$

$$\mathbf{Y}_P(t) = \frac{1}{2N\zeta}\int_{-\infty}^t \mathbf{f}_p^Y(t')\exp\left[-(t-t')/\tau_p\right]\mathrm{d}t' \; p = 2, 4, 6, 8, \ldots \quad (29b)$$

where

$$\tau_p = \frac{\zeta N^2 b^2}{2\pi^2 k_B T} \frac{1}{p^2} \quad p = 2, 4, 6, 8, \ldots \tag{30}$$

Using eqn (18), we also obtain

$$\left\langle X_{p\alpha}(t) X_{q\beta}(0) \right\rangle = \delta_{pq}\delta_{\alpha\beta} \frac{k_B T}{k_p} \exp\left(-t/\tau_p\right) \quad \text{for} \quad p, q = 0, 2, 4, 6, \cdots \tag{31a}$$

$$\left\langle Y_{p\alpha}(t) Y_{q\beta}(0) \right\rangle = \delta_{pq}\delta_{\alpha\beta} \frac{k_B T}{k_p} \exp\left(-t/\tau_p\right) \quad \text{for} \quad p, q = 2, 4, 6, \cdots \tag{31b}$$

$$\left\langle X_{p\alpha}(t) Y_{q\beta}(0) \right\rangle = 0 \quad \text{for all } p \text{ and } q \tag{31c}$$

(a) Relaxtion time

According to eqn (14), the longest characteristic relaxation (Rouse) time for the 2D linear polymer is therefore

$$\tau_{R,linear} = \tau_1 = \frac{\zeta N^2 b^2}{2\pi^2 k_B T} \tag{32}$$

Similarly, according to eqn (20), the longest characteristic relaxation time for the 2D ring polymer is

$$\tau_{R,ring} = \tau_2 = \frac{\zeta N^2 b^2}{8\pi^2 k_B T} \tag{33}$$

We thus see that the Rouse time of the 2D ring polymer is equal to one-fourth of that of the corresponding 2D linear polymer, i.e., $\tau_{R,ring} = \tau_{R,linear} / 4$, which is essentially the same as the 3D

Rouse model prediction for ring and linear polymers.[16]

(b) Mean-square chain end-to-end distance and ring diameter

Defining the chain end-to-end vector as $\mathbf{R}_{ete}(t) \equiv \mathbf{R}_N(t) - \mathbf{R}_0(t)$ for the linear polymer, we obtain from eqn (8a) that

$$\mathbf{R}_{ete}(t) = \mathbf{R}_N(t) - \mathbf{R}_0(t) = -4 \sum_{p=odd}^{\infty} \left[\mathbf{X}_p \cos(\frac{p\pi n}{N}) \right] \tag{34a}$$

$$\begin{aligned} \left\langle \mathbf{R}_{ete}(t) \cdot \mathbf{R}_{ete}(0) \right\rangle &= 16 \sum_{p;odd}^{\infty} \left[\left\langle \mathbf{X}_p(t) \cdot \mathbf{X}_p(0) \right\rangle \cos^2(\frac{p\pi n}{N}) \right] \\ &= 32 \sum_{p;odd}^{\infty} \left[\frac{k_B T}{k_P} \exp(-t/\tau_p) \right] \\ &= Nb^2 \sum_{p;odd}^{\infty} \frac{8}{\pi^2 p^2} \exp(-t/\tau_p) \end{aligned} \tag{34b}$$

$$\left\langle \mathbf{R}_{ete}^2 \right\rangle = \frac{8Nb^2}{\pi^2} \sum_{p;odd}^{\infty} \frac{1}{p^2} = Nb^2 \tag{34c}$$

where *p;odd* in the summation represents only the odd *p*-modes, i.e., $p = 1, 3, 5, 7 \cdots$.

Defining the ring diameter vector as $\mathbf{R}_d(t) \equiv \mathbf{R}_{n+N/2}(t) - \mathbf{R}_n(t)$ with $n = 1, 2, \cdots, N$ for the ring polymer, we obtain from eqn (9a) that

$$\mathbf{R}_d(t) = \mathbf{R}_{n+N/2}(t) - \mathbf{R}_n(t) = -4 \sum_{p=2,6,10,\ldots}^{\infty} \left[\mathbf{X}_p \cos(\frac{p\pi n}{N}) + \mathbf{Y}_p \sin(\frac{p\pi n}{N}) \right] \tag{35a}$$

$$\left\langle \mathbf{R}_d(t)\cdot\mathbf{R}_d(0)\right\rangle = 16\sum_{p=2,6,10,14,\ldots}^{\infty}\left[\left\langle \mathbf{X}_p(t)\cdot\mathbf{X}_p(0)\right\rangle\cos^2(\frac{p\pi n}{N})+\left\langle \mathbf{Y}_p(t)\cdot\mathbf{Y}_p(0)\right\rangle\sin^2(\frac{p\pi n}{N})\right]$$

$$= 32\sum_{p=2,6,10,14,\ldots}^{\infty}\left[\frac{k_BT}{k_P}\exp(-t/\tau_p)\right] \qquad (35b)$$

$$= Nb^2\sum_{p=2,6,10,14,\ldots}^{\infty}\frac{8}{\pi^2p^2}\exp(-t/\tau_p)$$

$$\left\langle \mathbf{R}_d^2\right\rangle = \frac{8Nb^2}{\pi^2}\sum_{p=2,6,10,14,\ldots}^{\infty}\frac{1}{p^2} = \frac{2Nb^2}{\pi^2}\sum_{p;odd}^{\infty}\frac{1}{p^2} = \frac{Nb^2}{4} \qquad (35c)$$

Therefore, the mean-square ring diameter of a 2D ring chain is equal to one-fourth of the mean-square chain end-to-end of the 2D linear analogue. This result is the same as that of the 3D Rouse model for ring and linear polymers.

(c) Mean-square chain radius of gyration

In addition, we can also find the mean-square radius of gyration $\left\langle R_g^2\right\rangle = \frac{1}{N}\sum_{n=1}^{N}\left\langle\left(\mathbf{R}_n-\mathbf{R}_G\right)^2\right\rangle$ with the center-of-mass position vector $\mathbf{R}_G = \frac{1}{N}\int_0^N \mathbf{R}_n\,dn$ for 2D ring and linear polymers. From eqn (8b), it is seen that $\mathbf{X}_0$ is equal to $\mathbf{R}_G$. We then derive the following expression for the mean-square radius of gyration for the 2D linear polymer.

$$\left\langle R_g^2 \right\rangle_{linear} = \frac{1}{N}\sum_{n=1}^{N}\left\langle \left(\mathbf{R}_n - \mathbf{R}_G\right)^2 \right\rangle$$
$$= \frac{1}{N}\sum_{n=1}^{N}\left\langle \left(\sum_{p=1}^{\infty}\left[2\mathbf{X}_p \cos(\frac{p\pi n}{N}) \right] \right)^2 \right\rangle$$
$$= \frac{4}{N}\sum_{p=1}^{\infty}\left[\left\langle \mathbf{X}_p^2 \right\rangle \int_0^N \mathrm{d}n \cos^2(\frac{p\pi n}{N}) \right] \qquad (36)$$
$$= 2\sum_{p=1}^{\infty}\left(\left\langle \mathbf{X}_p^2 \right\rangle \right)$$
$$= \frac{Nb^2}{\pi^2}\sum_{p=1}^{\infty}\frac{1}{p^2} = \frac{Nb^2}{6}$$

Similarly, we obtain the following result for the 2D ring polymer.

$$\left\langle R_g^2 \right\rangle_{ring} = \frac{1}{N}\sum_{n=1}^{N}\left\langle \left(\mathbf{R}_n - \mathbf{R}_G\right)^2 \right\rangle$$
$$= \frac{1}{N}\sum_{n=1}^{N}\left\langle \left(\sum_{p=even}^{\infty}\left[2\mathbf{X}_p \cos(\frac{p\pi n}{N}) + 2\mathbf{Y}_p \cos(\frac{p\pi n}{N}) \right] \right)^2 \right\rangle$$
$$= \frac{4}{N}\sum_{p=even}^{\infty}\left[\left\langle \mathbf{X}_p^2 \right\rangle \int_0^N \mathrm{d}n \cos^2(\frac{p\pi n}{N}) + \left\langle \mathbf{Y}_p^2 \right\rangle \int_0^N \mathrm{d}n \sin^2(\frac{p\pi n}{N}) \right] \qquad (37)$$
$$= 2\sum_{p=even}^{\infty}\left(\left\langle \mathbf{X}_p^2 \right\rangle + \left\langle \mathbf{Y}_p^2 \right\rangle \right)$$
$$= \frac{2Nb^2}{\pi^2}\sum_{p=even}^{\infty}\frac{1}{p^2} = \frac{Nb^2}{12}$$

It is thus seen that the mean-square radius of gyration of a 2D ring chain is equal to one-half that of the corresponding 2D linear chain. This is again the same as the 3D Rouse model prediction for ring and linear polymers.

(d) Diffusion coefficient

According to eqn (10a) for the 2D linear polymer, the dynamics of $\mathbf{X}_0$ (=$\mathbf{R}_G$) is governed by

$$\frac{\partial \mathbf{X}_0}{\partial t} = \frac{1}{2N\zeta}\mathbf{f}_0^X$$
$$\mathbf{X}_0(t) = \mathbf{X}_0(0) + \int_0^t \frac{1}{2N\zeta}\mathbf{f}_0^X(t')\mathrm{d}t' \tag{38}$$

Using eqn (12c), we arrive at

$$\left\langle X_{0\alpha}(t) - X_{0\alpha}(0)\right\rangle\left\langle X_{0\beta}(t) - X_{0\beta}(0)\right\rangle$$
$$= \left(\frac{1}{2N\zeta}\right)^2 \int_0^t\int_0^t \left\langle f_{0\alpha}(t')\, f_{0\beta}(t'')\right\rangle \mathrm{d}t'\mathrm{d}t'' = \frac{2k_BT}{N\zeta}\delta_{\alpha\beta}t \tag{39}$$

and thus

$$\left\langle \left(\mathbf{R}_G(t) - \mathbf{R}_G(0)\right)^2\right\rangle = \frac{4k_BT}{N\zeta}t \tag{40}$$

From the well-known Einstein equation for self-diffusivity, the center-of-mass diffuison coefficient D_G for the 2D linear polymer is therefore found to be

$$D_{G,linear} = \lim_{t\to\infty}\frac{\left\langle \left(\mathbf{R}_G(t) - \mathbf{R}_G(0)\right)^2\right\rangle}{4t} = \frac{k_BT}{N\zeta} \tag{41}$$

Similarly, based on eqns (16a) and (16c), we find for the 2D ring polymer that

$$D_{G,ring} = \lim_{t\to\infty}\frac{\left\langle \left(\mathbf{R}_G(t) - \mathbf{R}_G(0)\right)^2\right\rangle}{4t} = \frac{k_BT}{N\zeta} \tag{42}$$

Therefore, the center-of-mass diffuison coefficient of the 2D ring polymer is equal to that of the 2D linear analogue, which appears to be the same as the corresponding 3D Rouse model prediction.

Below summarized are the primary structural and dynamical properties predicted by the

Rouse model for the 2D linear and ring polymers in comparison to the corresponding 3D analogues.

$\left\langle R_{\mathrm{ete}}^2 \right\rangle / \left\langle R_{\mathrm{d}}^2 \right\rangle$	Linear Polymer ($\left\langle R_{\mathrm{ete}}^2 \right\rangle$)	Ring Polymer ($\left\langle R_{\mathrm{d}}^2 \right\rangle$)
2D	Nb^2	$\frac{Nb^2}{4}$
3D	Nb^2	$\frac{Nb^2}{4}$
$\left\langle R_{\mathrm{g}}^2 \right\rangle$	Linear Polymer	Ring Polymer
2D	$\frac{Nb^2}{6}$	$\frac{Nb^2}{12}$
3D	$\frac{Nb^2}{6}$	$\frac{Nb^2}{12}$
τ_{Relax}	Linear Polymer	Ring Polymer
2D	$\frac{\zeta N^2 b^2}{2\pi^2 k_B T}$	$\frac{\zeta N^2 b^2}{8\pi^2 k_B T}$
3D	$\frac{\zeta N^2 b^2}{3\pi^2 k_B T}$	$\frac{\zeta N^2 b^2}{12\pi^2 k_B T}$
D_{G}	Linear Polymer	Ring Polymer
2D ($D_{\mathrm{G}} = \lim_{t\to\infty} \frac{\left\langle \left(\mathbf{R}_G(t) - \mathbf{R}_G(0)\right)^2 \right\rangle}{4t}$)	$\frac{k_B T}{N\zeta}$	$\frac{k_B T}{N\zeta}$
3D ($D_{\mathrm{G}} = \lim_{t\to\infty} \frac{\left\langle \left(\mathbf{R}_G(t) - \mathbf{R}_G(0)\right)^2 \right\rangle}{6t}$)	$\frac{k_B T}{N\zeta}$	$\frac{k_B T}{N\zeta}$

Supplementary Note 3

In comparison to those of the corresponding 3D systems, the key distinctive feature in the MSDs of both ring and linear chains in 2D confined melt systems is that chains in the 2D systems tend to move as a whole with their monomers in a concerted manner. This characteristic is closely associated with the following distinct diffusive dynamics of the 2D melt systems compared to the corresponding 3D systems: (a) the monomeric MSDs [$g_1(t)$ and $g_2(t)$] are not much larger than $g_3(t)$ at short-to-intermediate time scales for the 2D systems, which is in sharp contrast to those for the 3D system, (b) $g_2(t)$ and $g_3(t)$ for the 2D systems cross each other at a much early time before reaching the $\left\langle R_g^2 \right\rangle$-length scale, unlike for the 3D system, (c) the overall faster diffusive motion of the 2D chains in comparison to the corresponding 3D analogues, which is also influenced by the absence of complex topological constraints between chains (i.e., interchain entanglement and mutual ring threading) in the 2D systems, and (d) the significantly diminished dynamic role of the chain ends of the linear polymer results in the overall quantitatively similar dynamic behaviors of the MSDs [$g_1(t)$, $g_2(t)$, and $g_3(t)$] between 2D ring and linear chains, in spite of the difference in their intrinsic molecular architectures, which is in stark contrast to those for the 3D system.

We further note that the general diffusive mechanism of chains in the 2D systems is quite distinctive from that of the 3D systems; i.e., 2D chains, with frequent stretching out or coiling of the chain-end segments, often fold back to their previous chain contour due to the spatial blockage by other adjacent chains, leading to a narrow, extended double-stranded local segmental conformation.

Description of supplementary movies

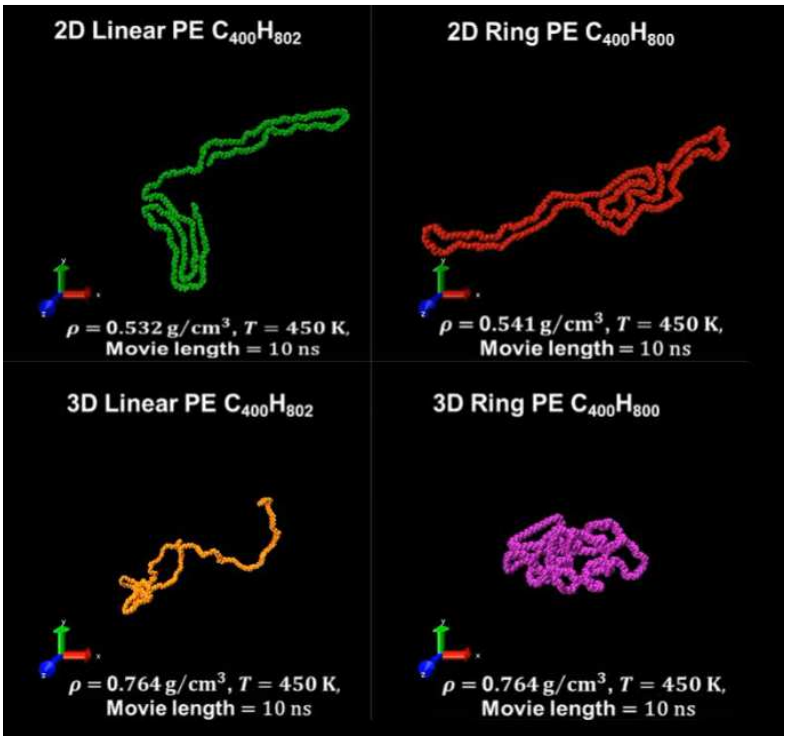

Movie S1 Chain dynamics for 2D and 3D L_400 PE melts (left) and R_400 PE melts (right) from atomistic molecular dynamics simulations.

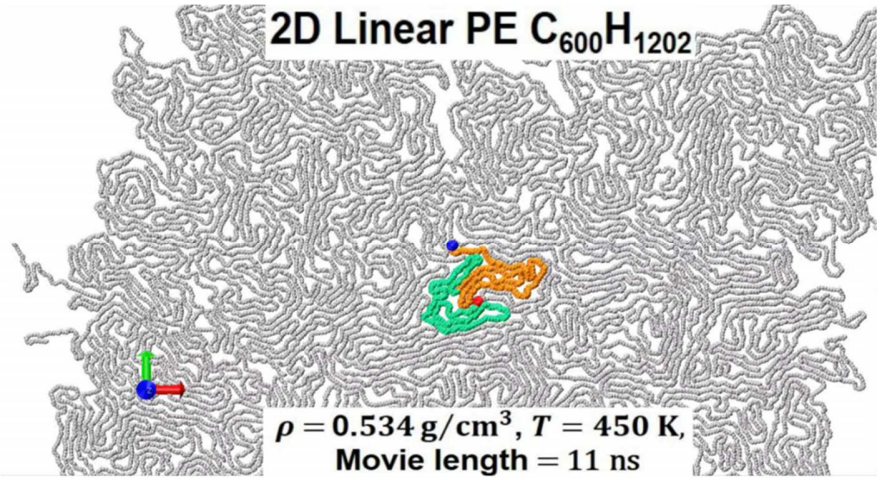

Movie S2 Dynamics of a randomly selected chain for 2D L_600 PE melt from atomistic molecular dynamics simulations.

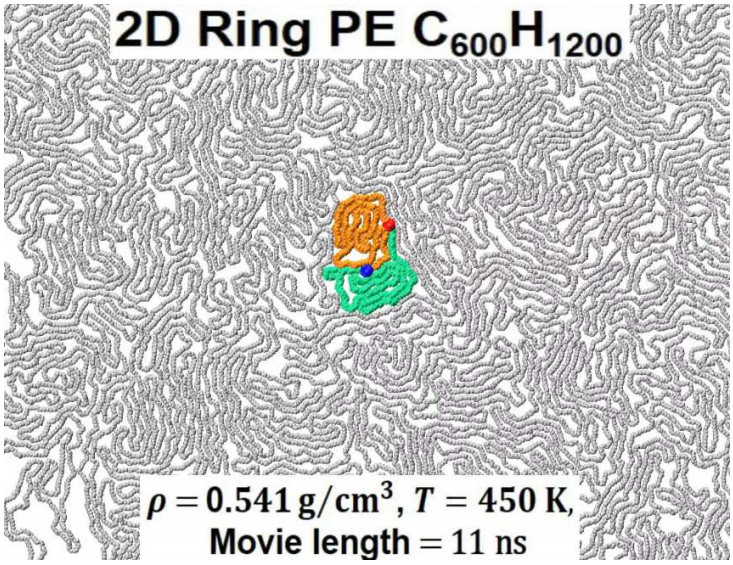

Movie S3 Dynamics of a randomly selected chain for 2D R_600 PE melt from atomistic molecular dynamics simulations.

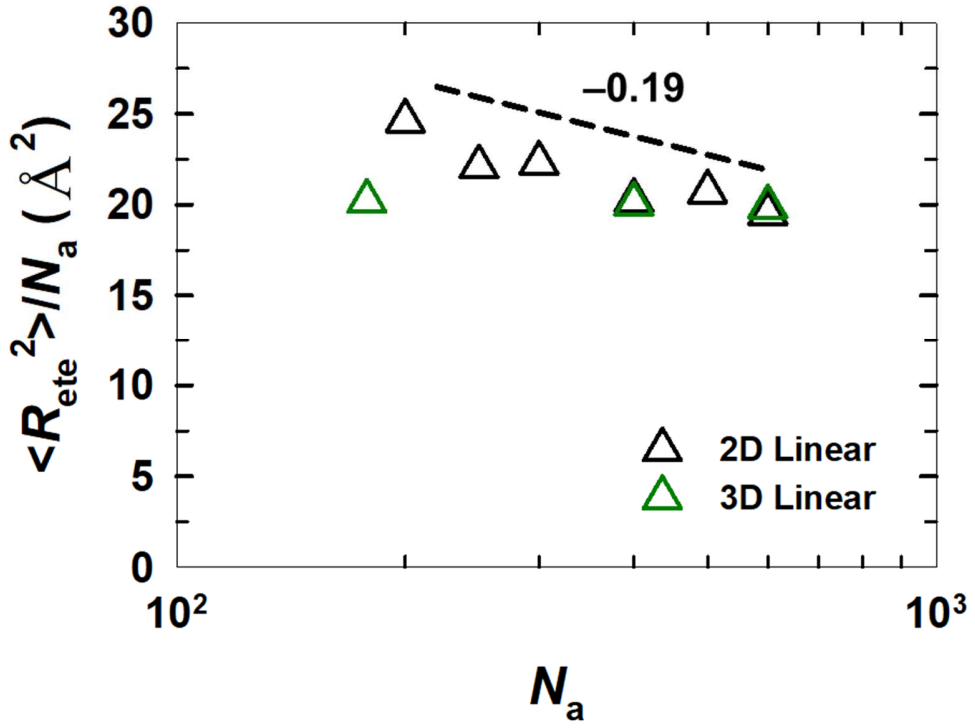

Fig. S1 Rescaled mean-square chain end-to-end distance $< R_{ete}^2 > / N_a$ of polymer chains as functions of chain length for 2D (black) and 3D (green) linear PE melts on a log–log plot. The data for the 2D and 3D linear systems were obtained from ref. 15.

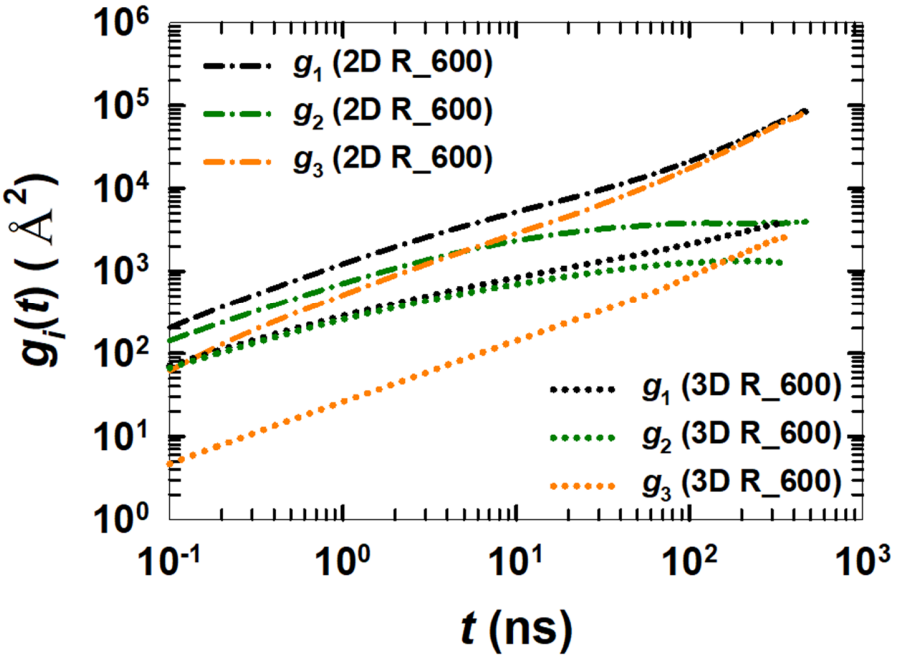

Fig. S2 The MSDs for 2D (dash-dot lines) and 3D (dotted lines) R_600 PE melts: MSDs averaged over all the monomers of a chain [$g_1(t)$; black], MSDs of monomers with respect to the center of mass of the chain [$g_2(t)$; dark green], and MSDs of the center of mass of the chain [$g_3(t)$; orange].

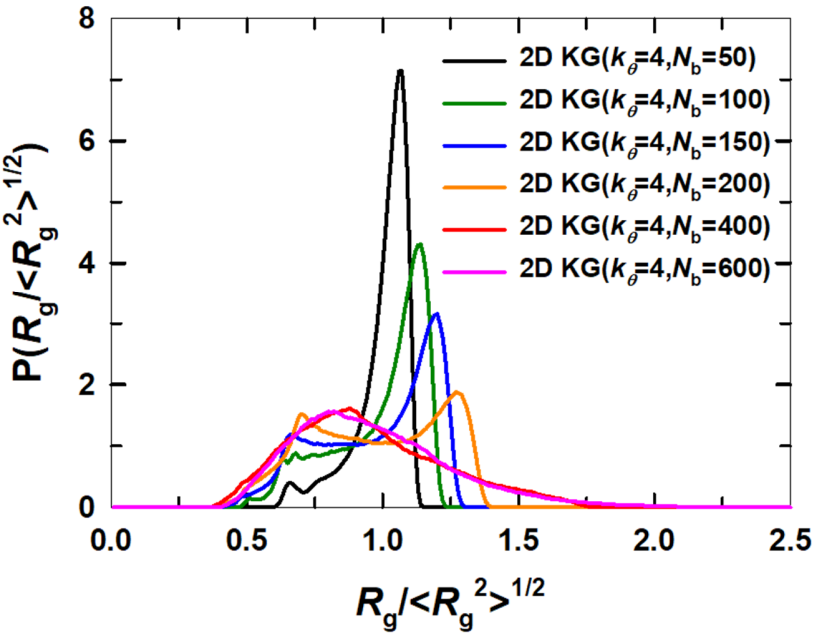

Fig. S3 Probability distribution function of $R_g / \langle R_g^2 \rangle^{1/2}$ as function of chain length for 2D KG ring melts with $k_\theta = 4$.

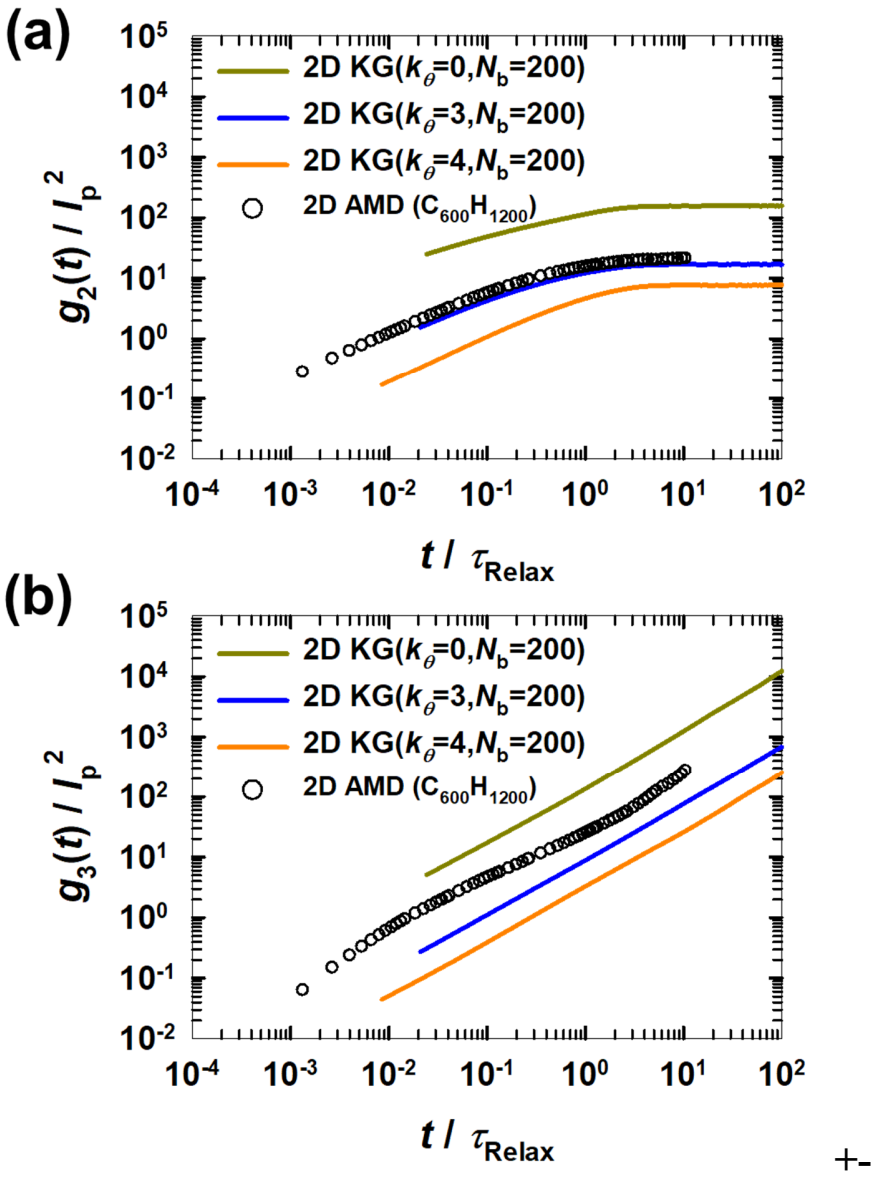

Fig. S4 (a) MSD of monomers with respect to center of mass of the chain [$g_2(t)$] and (b) MSD of the chain center-of-mass [$g_3(t)$] rescaled as $g_i(t)/l_p^2$ as a function of t/τ_{Relax} for ring polymers in 2D AMD system of R_600 (black circles) and 2D KG systems with N_b = 200 and k_θ = 0 (dark-yellow line), k_θ = 3 (blue line), and k_θ = 4 (orange line).

References

1 S. Nosé, *Mol. Phys.*, 1984, **52**, 255-268.

2 S. Nosé, *J. Chem. Phys.*, 1984, **81**, 511.

3 W.G. Hoover, *Phys. Rev. A*, 1985, **31**, 1695-1697.

4 M. Tuckerman, B.J. Berne and G.J. Martyna, *J. Chem. Phys.*, 1992, **97**, 1990-2001.

5 J.I. Siepmann, S. Karaborni and B. Smit, *Nature*, 1993, **365**, 330-332.

6 P. van der Ploeg and H. J. C. Berendsen, *J. Chem. Phys.*, 1982, **76**, 3271-3276.

7 W. L. Jorgensen, J. D. Madura and C. J. Swenson, *J. Am. Chem. Soc.*, 1984, **106**, 6638-6646.

8 J. D. Weeks, D. Chandler and H. C. Anderson, *J. Chem. Phys.*, 1971, **54**, 5237-5247.

9 K. Kremer and G. S. Grest, *J. Chem. Phys.*, 1990, **92**, 5057-5086.

10 R. Faller, A. Kolb and F. Müller-Plathe, *Phys. Chem. Chem. Phys.*, 1999, **1**, 2071-2076.

11 R. Faller, F. Müller-Plathe and A. Heuer, *Macromolecules*, 2000, **33**, 6602-6610.

12 B. Duplantier, *J. Stat. Phys.*, 1989, **54**, 581-680.

13 A. N. Semenov and A. Johner, *Eur. Phys. J. E*, 2003, **12**, 469-480.

14 J. Kumaki, *Polym. J.*, 2016, **48**, 3-14.

15 J. Kim, J. M. Kim and C. Baig, *Polymer*, 2021, **213**, 123308.

16 G. Tsolou, N. Stratikis, C. Baig, P. S. Stephanou and V. G. Mavrantzas, *Macromolecules*, 2010, **43**, 10692-10713.